JOURNAL OF NEUROTRAUMA 25:1027–1037 (August 2008)

DOI: 10.1089/neu.2007.0473

Macro-Architectures in Spinal Cord Scaffold Implants Influence Regeneration

Darice Y. Wong,[1] Jean-Christophe Leveque,[2] Hunter Brumblay,[2] Paul H. Krebsbach,[1] Scott J. Hollister,[1] and Frank LaMarca[2]

Abstract

Biomaterial scaffold architecture has not been investigated as a tunable source of influence on spinal cord regeneration. This study compared regeneration in a transected spinal cord within various designed-macro-architecture scaffolds to determine if these architectures alone could enhance regeneration. Three-dimensional (3-D) designs were created and molds were built on a 3-D printer. Salt-leached porous poly(ε-caprolactone) was cast in five different macro-architectures: cylinder, tube, channel, open-path with core, and open-path without core. The two open-path designs were created in this experiment to compare different supportive aspects of architecture provided by scaffolds and their influence on regeneration. Rats received T8 transections and implanted scaffolds for 1 and 3 months. Overall morphology and orientation of sections were characterized by H&E, luxol fast blue, and cresyl violet staining. Borders between intact gray matter and non-regenerated defect were observed from GFAP immunolabeling. Nerve fibers and regenerating axons were identified with Tuj-1 immunolabeling. The open-path designs allowed extension of myelinated fibers along the length of the defect both exterior to and inside the scaffolds and maintained their original defect length up to 3 months. In contrast, the cylinder, tube, and channel implants had a doubling of defect length from secondary damage and large scar and cyst formation with no neural tissue bridging. The open-path scaffold architectures enhanced spinal cord regeneration compared to the three other designs without the use of biological factors.

Key words: immunohistochemistry; *in vivo* studies; neural injury; polycaprolactone; regeneration; scaffold architecture; traumatic spinal cord injury

Introduction

THE PURPOSE OF THIS STUDY was to investigate the effects of varied implant architectures on spinal cord (SC) regeneration. Most studies of chronic spinal cord injury (SCI) repair have employed tubes or channels and combined their material implant with bio-active factors (Hadlock and Sundback, 2006; Nomura et al., 2006; Zhang et al., 2005). There have been no explicit comparisons of architectures which take into account how scaffold material is distributed with respect to white and gray matter distribution, though their physical organization is integral to the functions carried out by the SC.

Treatments for SCI under investigation include use of trophic factors, antibodies, enzymes, stem cells, Schwann cells, or olfactory ensheathing cells (Barnett and Riddell, 2007) to help rebuild the tissue through re-myelination, axonal guidance, or prevention of secondary damage (Hadlock and Sundback, 2006; Nomura et al., 2006; Zhang et al., 2005). Cell transplantation and injected factor therapies under investigation may be limited to small injuries, as survival of injected cells and residence time of injected factors is often quite low (Friedman et al., 2002). If the injury is too large, or in a chronic stage with a large area of secondary damage, a material scaffold is useful for increasing cell survival and localizing cells or biologic factors to the target area (Friedman et al., 2002; Tate et al., 2002).

Several biomaterials have been investigated with varying architectures and mechanical properties, aimed at delivering cells or trophic factors to the injured SC and guiding regeneration in a longitudinal direction (Bakshi et al., 2004; Carone and Hasenwinkel, 2006; Flynn et al., 2003; Gelain et al., 2007; Horn et al., 2007; Houle and Ziegler, 1994; Huang et al., 2005; Li et al., 2006; Nomura et al., 2006; Stokols et al., 2006; Teng et al., 2002). Microgrooves in biomaterials play an important role in contact guidance for neurites *in vitro*. Studies of chick embryo neurons *in vitro* revealed a lower limit on feature size for neurite alignment to be a 2-μm groove depth (Clark

Departments of [1]Biomedical Engineering and [2]Neurosurgery, University of Michigan, Ann Arbor, Michigan.

et al., 1990). This size range was found to be specific for neurites when compared to fibroblasts and endothelial cells (Clark et al., 1991). An upper limit for neurite alignment *in vitro* exists around 10—30 μm (Miller et al., 2002; Goldner et al., 2006). In fact, the narrower the ridge (while still above single microns) the more concentrated the focal adhesions are to the ridge, thus aligning the cytoskeleton with the grooved features (Ito, 1999). Other researchers have shown *in vivo* that 20 μm diameter collagen micro-filament bundles integrated into SC tissue and improved functional outcomes when aligned longitudinally (Yoshii et al., 2003), in contrast to the poorer performance of perpendicularly oriented fibers (Yoshii et al., 2004).

Thus far there have been no *in viv*o comparisons of topographical features and sizes. However the small nuances in feature size influences found *in vitro* with single cell cultures could well be lost when transferred to *in vivo* studies. Macroscale architecture was the focus of this study, thus microscale topography was fixed based on the studies outlined above. When micro-scale grooves (microgrooves), were incorporated into scaffolds, they were uniformly in the range of 30—50 μm with V-shaped profile; thus, the grooves and ridges were of tapered width. These grooves, an artifact of the mold building process, have been controlled to run longitudinally.

While micro-architectural contact guidance is important, there have also been indications that macro-scale architecture could play a role. One notable study demonstrated tissue bridges with axonal regeneration through a tube containing no fillers (Tsai et al., 2004), something other studies using entubulation could not show. This result was possibly a result of the micro-features of the material, a hydrogel with a spongy, porous or gel-like inner wall, compared to the materials used by others previously. This suggests the possibility that a material scaffold could support regeneration without the use of biologics and that altering the mechanical properties, which also changed the micro-architecture of the material, could affect the degree of regeneration. Furthermore, these researchers report that an increase in surface area from a hollow channel to a tubes-within-channels (TWC) design with four small inner tubes increases functional recovery and regeneration with out biologics (Tsai et al., 2006). This may seem contrary to other reports in which the surface area is much greater than the TWC design, such as microporous oriented channels which do not support regeneration (Hurtado et al., 2006). However, the change in surface area also changes the macro-architecture. We propose that not just the surface area, but the structure of the surfaces in relation to the anatomy of the SC may play a role in the regeneration.

The organization and reconnection of different tracts in the SC are important to functional recovery. For example, lateral and ventral corticospinal tracts are most important to recovery of locomotor function, while sparing of dorsal tracts provide less improvement (Kaegi et al., 2002; Mori, 1992; Noga et al., 1991; Schucht et al., 2002). When evaluating SCI in patients and their potential treatments, these types of anatomical distinctions have a great effect on the degree of functional recovery.

Various injury models have been used to study different aspects of injury and regenerative capacity. Contusion, hemisection, and complete transection are the most common models (Hadlock and Sundback, 2006; Nomura et al., 2006; Zhang et al., 2005). While each of the models has reproducible effects, it is more difficult in the contusion and hemisection models to determine if recovery is due to sparing and compensatory sprouting or new regeneration. Though contusions and hemisection models can be more clinically relevant, in cases where proof of concept and proof of regeneration is needed, the complete transection model is often useful, and is employed in this study.

Newly severed axons have regenerative capacity in the first few days but meet with restrictive environments such as myelin inhibitory factors and a quickly growing glial scar, which prevent axonal extension and complete regeneration to their original targets (Busch and Silver, 2007; Maier and Schwab, 2006; Schwab et al., 2006; Schwab, 2002). Different neurotrophic factors (Thoenen, 1991) are being investigated to make the injured environment more permissive to axonal regeneration (Barritt et al., 2006; El Maarouf et al., 2006; Novikova et al., 2003). The local balance of permissive and inhibitory factors should be tipped toward permissive (Jones et al., 2003). While bio-active factors will indeed play a strong role in SC regeneration, the architecture of implant material may play an important, and more easily controlled role as well.

This study has developed a method of manufacturing SC implants with very specific and varied designs that take into account white matter tracts. These new SC implant designs were compared to single and multiple channel architectures as well as a randomly porous cylindrical sponge.

The novel designs were conceived to provide surface area in key locations with grooves to direct growth while decreasing the barriers which might be presented by designs like multi-channeled scaffolds (Nomura et al., 2006) or cylindrical sponges (Patist et al., 2004). In fact, the new designs actually have less total longitudinal surface area than the other designs. Instead, they take advantage of the circumferential location of the white matter and the early secondary death of the gray matter. The new designs in this study have an open path for the lateral funiculi where the corticospinal tracts descend, while one contains a central core to provide an added surface for guidance of nerve fibers from that region. In a typical injury the center of the cord dies first, leaving the exterior white matter tracts to cave in, resulting in a narrowing at the defect site (Maier and Schwab, 2006; Schwab et al., 2006). The open-path scaffold with a core was designed to support the white matter tracts from the center. This is in contrast to the tube, channel, and cylinder designs with surfaces and obstructions in various locations as well as entubulation methods, which provide surface contact guidance from the outside of the cord. The cylindrical core present in one open-path design is suspended in the center of the defect by fins from the top and bottom shells (Fig. 1). In order to maintain a consistent implantation method, no entubulation was used. Instead, architectures with random or contrasting support were designed as comparisons.

The open-path designs allowed extension of myelinated fibers along the length of the defect both exterior to and inside the scaffolds and maintained their defect size over 3 months. In contrast, the cylinder, tube, and channel implants had a doubling of defect length from secondary damage and large scar and cyst formation with no neural tissue bridging. The benefits of the open-path designs could be due only to

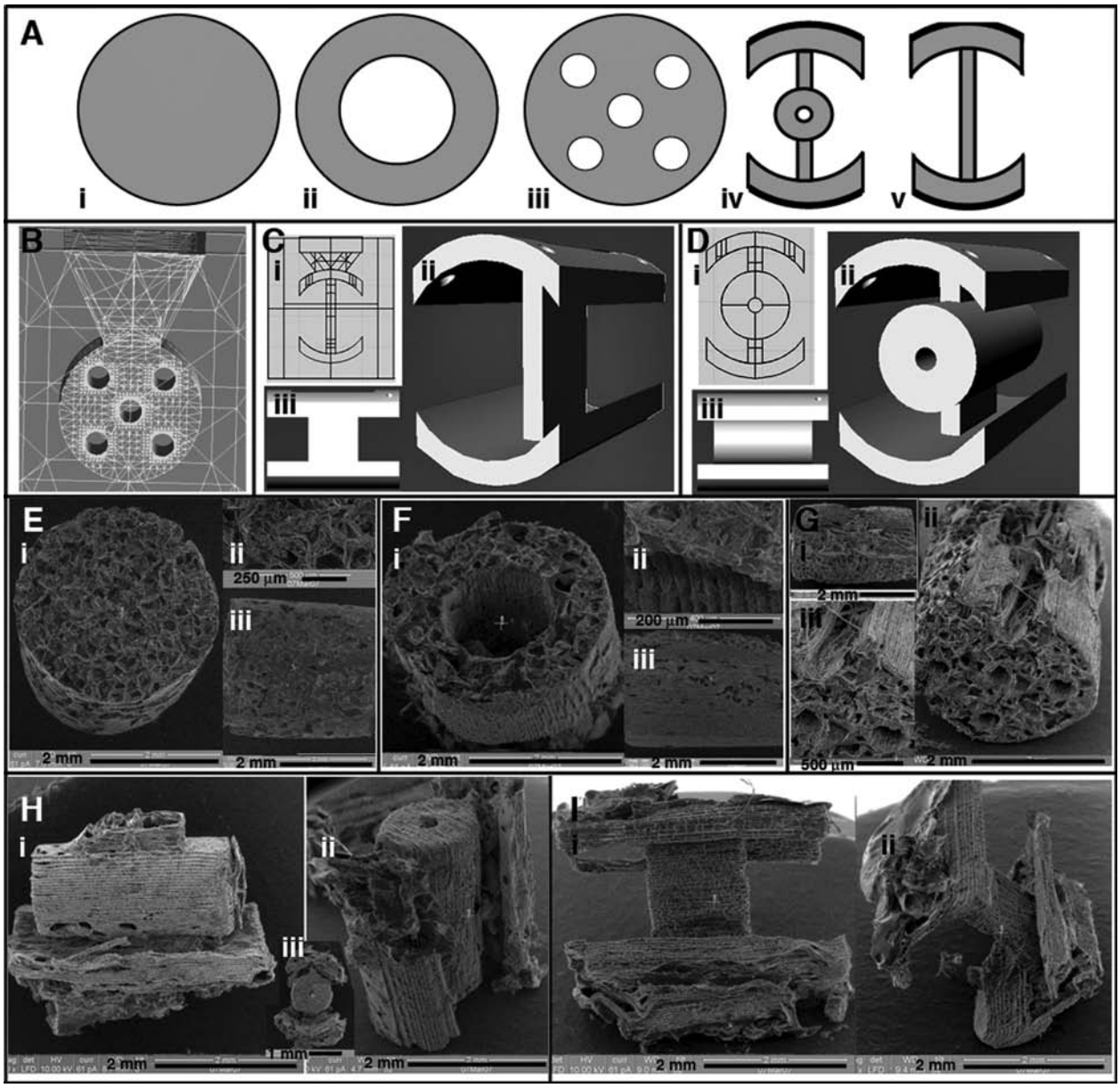

FIG. 1. Design and fabrication of macro-architectures for spinal cord implants. (**A**) Axial view of designs for cylinder (**i**), tube (**ii**), channel (**iii**), open-path with core (**iv**), and open-path without core (**v**). (**B**) Wireframe view of a mold for the channel design, a funnel is built into the top through which salt and polymer are poured to fill the mold. (**C**) The open-path without core mold design with polymer and salt inlet (**i**), oblique view (**ii**) and side view (**iii**). (**D**) The open-path with core design (**i**), oblique view (**ii**) and side view (**iii**). SEM micrographs for cylinder (**E**), tube (**F**), channel (**G**), open-path with core (**H**), and open-path without core (**I**) scaffolds after fabrication.

differences in macro-architecture, as material and microarchitecture were the same in all implants and no biological factors were used.

Methods

Scaffold Design and Fabrication

Implants were made of PCL (50,000 kDa MW; Solvay Chemicals Inc., Houston, TX), dissolved in acetone, (13% wt.) and 180—250 μm sieved salt crystals were used for porogen leaching. The general shape and size of the implants was a 4-mm-long cylinder with a 2.8-mm diameter. Five designs were used: cylinder, hollow tube, five-channel, open-path with core, and open-path with no core (Fig. 1A). Within the walls of each macro-design (gray areas in Fig. 1A), the implants were given a porous structure by salt leaching. Briefly, salt was poured into the molds, then solvent-dissolved PCL was injected through ports into the mold using a 30-gauge syringe needle multiple times until the mold was filled with PCL. All the salt crystals were packed prior to polymer injection and in contact with each other, forming random connections between the resulting pores. After polymer injection and solvent evaporation, all the salt was removed by soaking the scaffold in 70% ethanol, leaving crystal-shaped

pores where the salt crystals were. The complete removal of the salt, evidenced by pliability of the scaffold and translucence in water, further supports that the pores are interconnected throughout. The random organization and crystalline shape of the pores can be seen in scanning electron microscopy (SEM) images (Fig. 1). While these salt-generated pores do not uniformly traverse the entire length of the scaffolds, channels and other designed architectures can be specifically controlled with the design of the molds. Thus, the use of salt and designed molds creates two layers of porosity.

To achieve the intricate architectures, implants were designed in Rhinoceros software (McNeel North America, Seattle, WA), and wax molds were built on a 3D Solidscape printer (Solidscape Inc., Merrimack, NH; Fig. 1B—D). To impart longitudinal microgrooves, molds were built sideways with a funnel on top for pouring in salt and the polymer (Fig. 1B). Cylinder design implants were made in Teflon molds packed with salt and had no microgrooves (Fig. 1E). Microgrooves are an artifact of the layer-by-layer mold printing process. The programmed layer thickness was set to 38.1 μm. A groove is generated in the z-direction between each layer in the mold. The grooves are then transferred in the casting process to the actual polymer scaffold (Fig. 1F—I). The excess polymer was trimmed from each implant, and wax was dissolved in Bio-act (Solidscape Inc. Merrimack, NH). The Bio-act and salt particles were cleaned out with several washes of

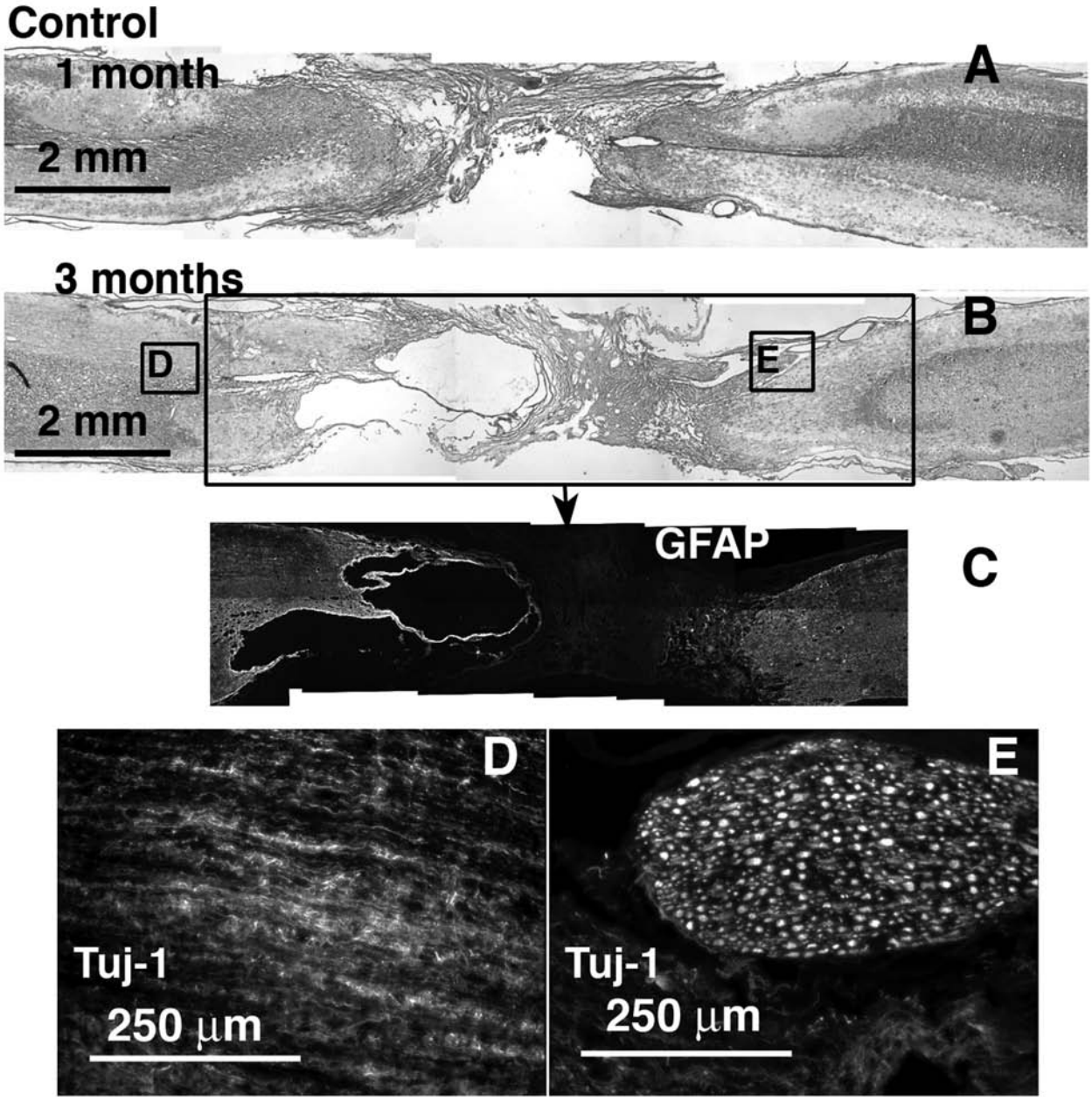

FIG. 2. Control defect, no scaffold implant, at 1 and 3 months, H&E stained and immunolabeled. Caudal end is always to the right. (**A**) 1 month H&E stained. (**B**) 3 months H&E stained section with corresponding regions (boxed) immunolabeled for GFAP (**C**), and Tuj-1 (**D,E**).

70% ethanol and agitation, and implants were stored sterilized in fresh 70% ethanol. Prior to surgery, implants were transferred to sterile saline.

PCL is a biocompatible polymer that degrades by hydrolysis. We have shown its biocompatibility is greater in the rat brain compared with its highly used family member, PLGA (Wong, Hollister, et al., 2007). It is easily processed to have the desired architectures for this study. The high molecular weight chosen here ensures that the architecture, the focal point of this study, is maintained for the duration of the experiments. In future studies it may be desirable to have a more quickly degrading scaffold. This material can be used with a lower molecular weight or surface treatment to increase its degradation rate while its degradation products, and any tissue reaction to them, will be maintained. When PCL is solvent cast with porogen leaching, the resulting scaffold is spongy and pliable, yet can still be surgically manipulated.

The total longitudinal surface areas for each geometrical design, not calculating for surface roughness and micropores, were as follows (in mm^2): tube, 60.3; channel, 66.6; cylinder, 37.7; open-path with core, 48.3; and open-path without core, 44.8. The open path designs have nearly 30% less surface area than the tube and channel, and roughly 20% greater surface area than the cylinder.

Surgical Implantation

Female Sprague Dawley rats (200—250 g) were anesthetized with isofluorane and intubated. Following a laminectomy from T7 to T9, SCs were completely transected at T8 with a 2-mm-long removal of tissue. With subsequent tissue retraction, the gap was 4 mm long. Control groups received no implant. Implants were sutured to proximal and distal stumps, and then covered with Durepair (Medtronic, Minneapolis, MN). Daily bladder expression, antibiotics, and husbandry attention were administered as needed. Each time point and group contained $n = 3$ replicate animals. Deaths reduced the number of rats in the channel group to one rat at 1 month. Rats were sacrificed at 1 and 3 months by transcardial perfusion. SCs were cryosectioned longitudinally for immunohistochemistry and staining onto gelatin coated slides. All surgery, post-surgical recovery and euthanasia were performed according to a protocol approved by the University of Michigan Committee on the Use and Care of Animals.

Histology and Immunohistochemistry

Stains and antibodies used were hematoxylin and alcoholic eosin (H&E), Luxol Fast Blue (LFB) (myelin stain) and Cresyl Violet (Nissl substance, neuron stain), rabbit anti-

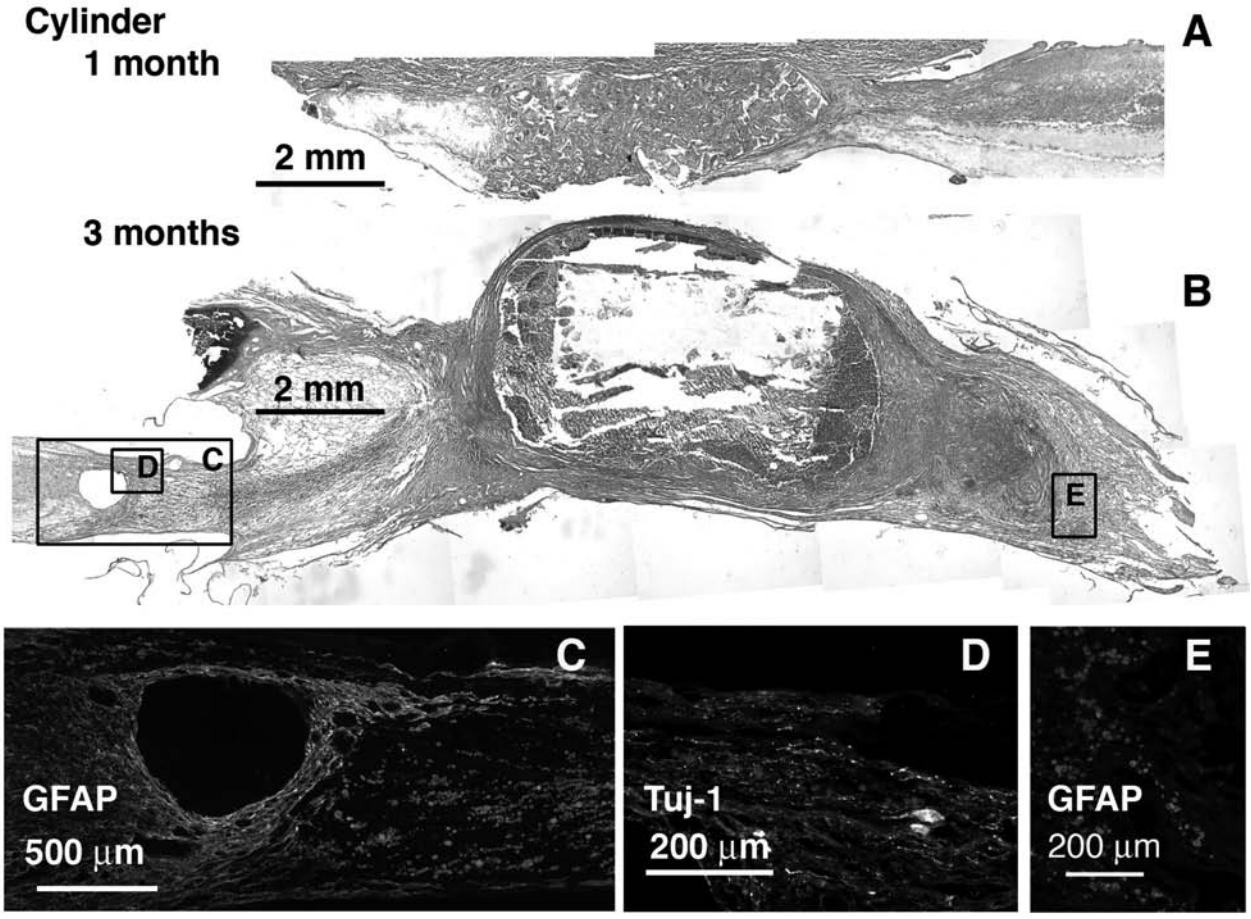

FIG. 3. Cylinder implant at 1 and 3 months, sagittal sections H&E stained and immunolabeled for GFAP and Tuj-1. Caudal end is always to the right. (**A**) 1 month H&E stained. (**B**) 3 months H&E stained with corresponding regions (boxed) immunolabeled for GFAP (**C,E**), and Tuj-1 (**D**).

GFAP for astrocytes (G9269 Sigma), mouse anti-Tuj-1 for axons (MMS-435P Covance, Berkeley, CA) with a Vecta-stain ABC kit (Vector Labs, Burlingame, CA), and biotinylated Alexa-488 (Invitrogen/Molecular Probes, Carlsbad, CA) for fluorescent visualization. Non-specific binding was blocked with 5% donkey serum and 3% bovine serum albumin (Jackson ImmunoResearch, West Grove, PA). Images were taken using a Spot camera and Spot Advanced software (Diagnostic Instruments, Sterling Heights, MI).

Statistical Analysis

Defect lengths were measured from serial sections labeled with GFAP to identify the extent of degeneration of the central core of gray matter. Because of the poor connectivity between some stumps of the control group and easy disruption during tissue handling, defect lengths for the control group were not measured (Fig. 2). Two-way analysis of variance (ANOVA) was carried out on defect length measurements with time and group as independent variables. Tukey's Least Significant Difference post-hoc analysis was used for multiple comparison between groups if significance levels were below $p = 0.05$.

For each animal at 3 months, multiple stained and labeled slides were evaluated to determine presence or absence for each animal with the following indications: H&E-stained tissue growth bridging the entire defect through or around the implant without break (tissue ingrowth and continuity), Luxol Fast Blue stained myelinated fibers with appropriate morphology extending into, across, or within the defect site (myelinated fibers), GFAP-labeled cells found within the defect site beyond the ends of the implant (astrocyte immigration), Tuj-1—labeled fibers within or around the defect site beyond the ends of the implant but not necessarily extending the entire length (axonal infiltration). With $n = 3$ for each group, not including the control, each assessment is given one "+" for each animal in which the quality was found on at least one slide. If none of the animals in that group qualified a "+", the entire group received one "-". These assessments are summarized in Table 1.

Results

From H&E staining and gross images, connectivity between the stumps was obtained in all implants to varying degrees. Much of the growth for the cylinder (Fig. 3), and tube and channel groups (Fig. 4) occurred along the outside of these implants. Much of the porous interior walls were filled with cellular debris, macrophages, and fibroblast-like cells as observed from H&E staining at 1 month (Figs. 3A and 4A,H). By the 3-month time point, several of these implants showed secondary cell death within and around them (Figs. 3B and 4B,I). A high degree of secondary death was evident in these three groups at both ends of the

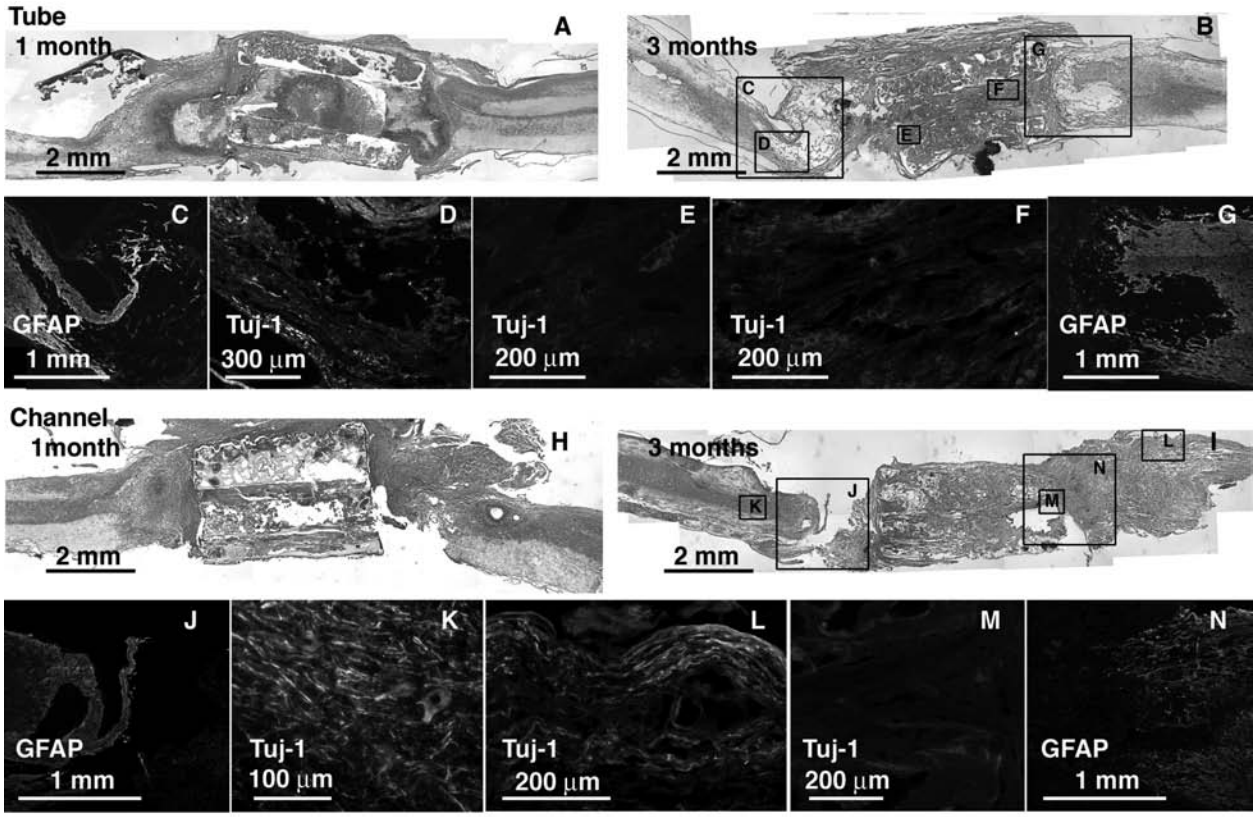

FIG. 4. Tube and channel implants at 1 and 3 months, sagittal sections H&E stained and immunolabeled for GFAP and Tuj-1. Caudal end is always to the right. (**A**) Tube section at 1 month H&E stained. (**B**) Tube section at 3 months H&E stained with correspondeing regions (boxed) immunolabeled for GFAP (**C,G**) and Tuj-1 (**D—F**). (C) Channel section at 1 month H&E stained. (D) Channel section at 3 months H&E stained with corresponding regions (boxed) immunolabeled for GFAP (**J,N**) and Tuj-1 (**K—M**).

injury. In particular, fibrous capsules formed around the cylinder design scaffolds after 3 months (Fig. 3B). GFAP antibodies labeled reactive astrocytes in intact SC and became diffuse and non-existent closer to and within the scaffold as tissue was degenerating and fibrous tissue had grown in Figure 4C,G,J,N. Tuj-1—labeled axons were found only in the remaining SC stumps (Fig. 4D,K,L). Oriented tissue within the tube and channels contained no axons (Fig. 4E,F,M).

In contrast, tissue grew interiorly along the entire length of both open-path implants and appeared well connected (Fig. 5). Because of the uncommon architecture of these scaffolds, diagrams of orientation and approximate planes of sectioning have been provided for each of the open-path de-

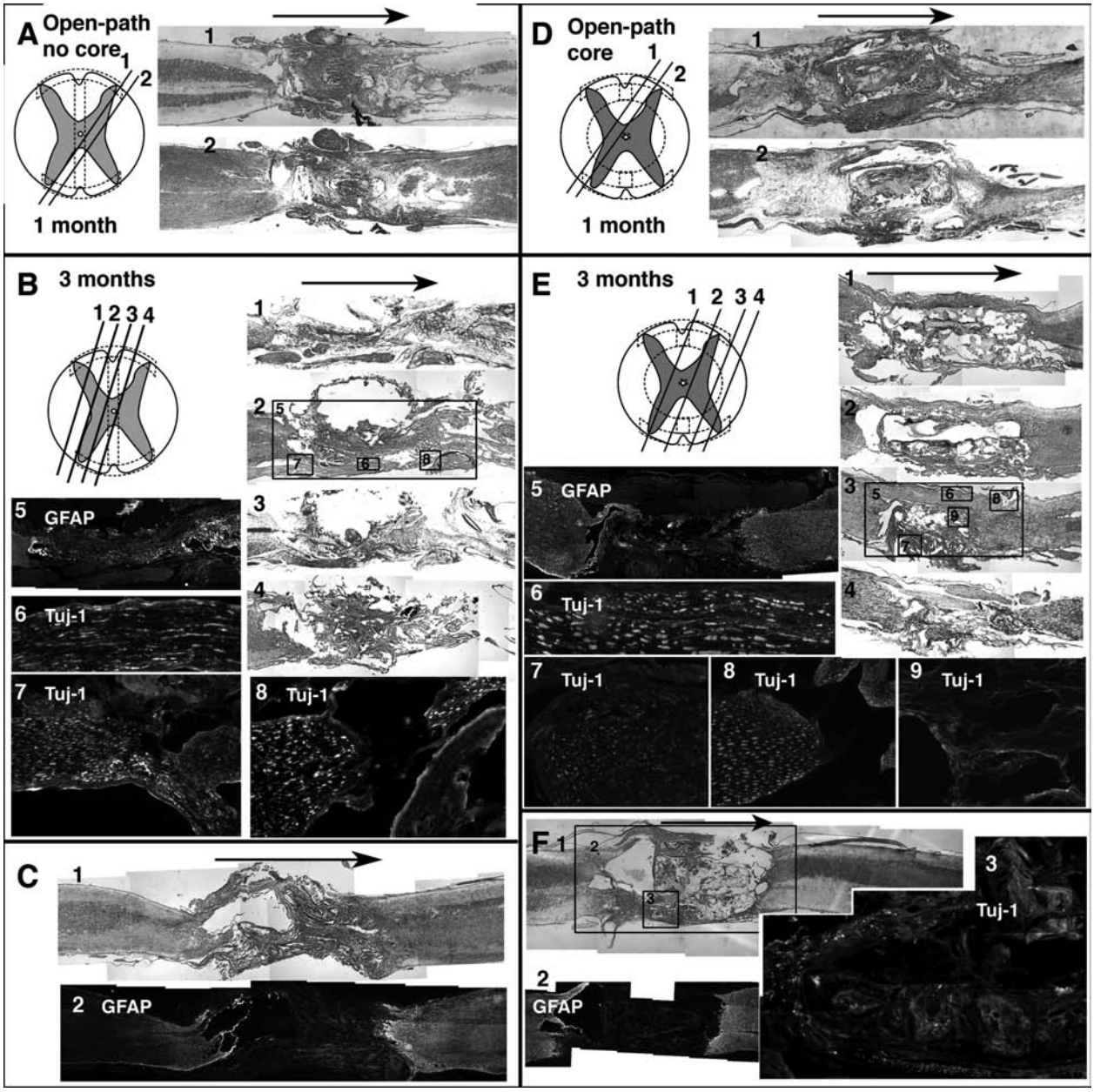

FIG. 5. Open-path designs with and without core, sagittal sections stained and immunolabeled. Arrows indicate rostral to caudal direction. (**A**) Two neighboring sections (orientation diagramed) from open-path without core at 1 month, H&E (**A-1**) and LFB (**A-2**) stained. (**B**) Four neighboring sections (orientation diagramed) from open-path without core at 3 months, H&E (**B-2, B-4**) and LFB (**B-1, B-3**) stained. Section shown in B-2 has corresponding regions (boxed) immunolabeled for GFAP (**B-5**) and Tuj-1 (**B-6, B-7, B-8**). (**C**) Two sections from a different animal from open-path without core 3-month group H&E (**C-1**) and LFB (**C-2**) stained. (**D**) Two neighboring sections (orientation diagramed) from open-path with core at 1 month, H&E (**D-1**) and LFB (**D-2**) stained. (**E**) Four neighboring sections (orientation diagramed) from open-path without core at 3 months, H&E (**E-1, E-2, E-3**) and LFB (**E-4**) stained. Section shown in E-3 has corresponding regions (boxed) immunolabeled for GFAP (**E-5**) and Tuj-1 (**E-6, E-7, E-8, E-9**). (**F**) Section from a different animal from open-path with core 3-month group H&E (**F-1**) stained with corresponding regions (boxed) immunolabeled for GFAP (**F-2**) and Tuj-1 (**F-3**).

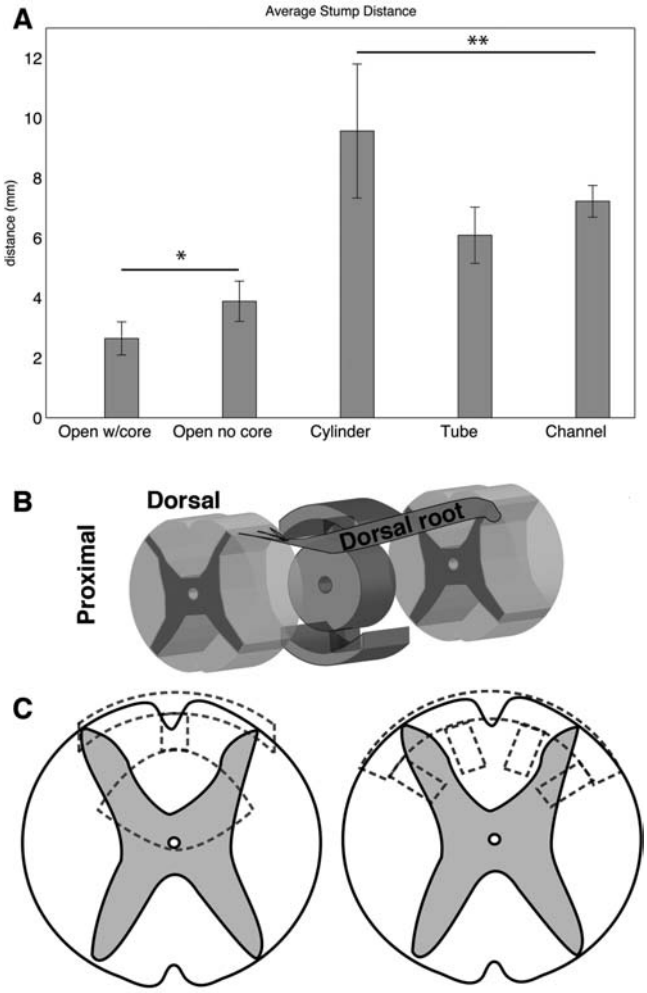

FIG. 6. Defect lengths and illustrations of possible interactions. (**A**) Average shortest distance between GFAP labeled intact cord stumps at 3 months, open-path designs (*) significantly lower than closed designs (**) ($p = 0.002$). (**B**) Illustration of open-path with core scaffold and its orientation within the defect. Nerve roots or regenerating white matter tracts from the lateral funiculus could possibly crawl along the inner core of the scaffold to bridge the defect. (**C**) Modified designs (dotted lines) could accommodate contusion (left) or hemisection (right) injury models while maintaining the same principles of complete transection designs.

signs along with images of neighboring sections (Fig. 5A,B,D,E). Histological results were consistent in replicate animals. An additional specimen is shown for each open-path design at the 3-month time point for comparison (Fig. 5C,F). The gross shape and size of the SC at the implant site was similar to uninjured areas of the cord, unlike the other three implant groups where large cysts and fibrotic tissue formed around the implants and their ends. There was less necrosis and scar tissue at both ends of the open-path implants, and neural tissue from both proximal and distal stumps entered and grew around the implants. Considerable tissue tracts along the periphery of the defect and the outside edges of the scaffolds contained intact Tuj-1—positive myelinated axonal fibers, though they never appeared to connect on the distal stump. Some of the thicker growths around the edges of the open-path designs could have been spinal nerves from either dorsal or ventral nerve roots, but instead of exiting the spinal canal, they merged with the scaffolds along the length of the defect before leaving the SC (Fig. 5). There were also Tuj-1—labeled axons within the open-path with core scaffolds, and fibers were observed straddling the edge of the bottom shell on both of its surfaces (Fig. 5F-3). The shell thickness was 200 μm.

Defect lengths measured from GFAP-labeled serial sections after 3 months *in vivo* showed that defects with open-path designs maintained their original lengths from the implant size of 4 mm (Fig. 6). Defects with the three closed designs had nearly a doubling of defect length from the original implant size ($p = 0.002$). As most secondary cell death occurs in the first few weeks, there was no significant difference in defect lengths over the two time points, 1 and 3 months ($p = 0.54$); thus, only 3- month data is reported.

Presence or absence of the different types of labeling or staining was assessed from all the sections for each replicate sample at 3 months. These qualitative assessments are summarized in Table 1 and provide a semi-quantitative summary of the histological data.

Discussion

The open-path designs both with and without core had a beneficial effect on the secondary injury progression by measure of the defect length. Overall morphological appearance of the cord specimens with these implants was more connected and less fibrous. Axonal regeneration was seen within

TABLE 1. THREE-MONTH ASSESSMENT OF HISTOLOGICAL DATA FROM EACH REPLICATE SAMPLE

	Tissue ingrowth and continuity (H&E)	*Myelinated fibers (LFB)*	*Astrocyte immigration (GFAP)*	*Axonal infiltration (Tuj1)*
Cylinder ($n = 3$)	−	−	−	−
Tube ($n = 3$)	+	−	−	+
Channel ($n = 3$)	+	−	+	+
Open-path without core ($n = 3$)	++	++	+	++
Open-path with core ($n = 3$)	++	+++	++	+++

Presence of staining or labeling within the defect site in one or more section of each replicate is indicated by a (+) for each replicate animal, whereas a (−) indicates none found. In the case of tissue ingrowth and continuity, fibrous tissue continuity between stumps and scaffold on both ends was assigned a (+), whereas discontinuity in all groups received a (−).

and around these implants, and particularly robust fibers were observed crossing the defects around the implants. These promising regenerative results were in complete contrast to the results in the other three designs whose defect lengths grew to 7 mm, and had no neural tissue regeneration across the defect site.

The completely transected and untreated control group has been unrepresented in data analysis in SC studies with 4-mm gap lengths (Nomura et al., 2006; Tsai et al., 2004, 2006) or left out completely from the study (Oudega et al., 2001) because of its lack of information. Untreated transections do not form good bridges, show no specific labeling of neural cell types, and are unsuccessful at regeneration. In terms of cell death, complete transection injuries have also shown a 40% tissue loss and a 0.79 _± 0.19 mm axonal die-back on both ends after 8 weeks (Oudega et al., 1999). One would expect the loss to be greater if tissue is also removed as in the case of our study and other similar studies. Thus, at best, one expects that the untreated control groups would have axonal die-back and tissue loss resulting in the 4-mm gap expanding to or in excess of 5.6 mm, likely greater. This is roughly the extent of our closed designs and that of the reported gap width of Tsai et al. (2004), ranging from 6 to 8 mm. These examples indicate that the open-path designs do improve regeneration over the other designs and over no treatment at all.

To further differentiate the two open-path designs, the implant with a central core had more robust nerve fiber extension across the defect site both around the outside of the implant and within the scaffold itself. The design without a core showed only bundles of fibers along the outside. Though not statistically significant, the open-path with core implant even showed a decrease in defect length, indicating some regeneration of the central region of the SC.

Though many nerve fibers were seen crossing the open-path scaffolds, it is possible that they were not newly regenerated fibers. Because the open-path designs were open rather than closed like the other three, there was space for nerve roots to potentially merge into the defect site prior to their exit (Fig. 6B). It is possible that these nerve roots served a protective role for the remaining cord, which could have prevented enlargement of the defect length. One of the most promising treatments for SCI currently is transplantation of peripheral nerve grafts (Houle et al., 2006; Kuo et al., 2007; Levi et al., 2002). Specifically, after a preconditioning injury, the Schwann cells of these grafts have been shown to migrate from the graft and myelinate the axons of injured SC (Dinh et al., 2007; Fukunaga et al., 2004). If those nerve fibers crossing the defect of the open-path designs were indeed uninjured spinal roots which became physically engaged in the defect along the scaffolds, their proximity and activation due to the injury could have promoted some neuroprotection. This type of interaction between the native peripheral nervous system and the injured SC would be impossible with entubulation methods, which enclose and protect the SC from exterior perturbations. Still the spared spinal nerve roots cannot account for the un-bundled and disorganized axonal growth found within the open-path with core scaffolds (Figs. 5E-7, 5E-9, and 5F-3).

The open-path with core design slightly out-performed the open-path without a core. The difference between the two designs is the central cylindrical core. The core could have provided an additional surface for guiding white matter tracts from a convenient position in the inside of the cord, as intended.

The three closed designs were unsuccessful at providing an environment conducive to regeneration, even though both the tube and the channel design had greater surface areas than the open-path designs. The cylinder implant resulted in extreme defect enlargement and fibrous tissue encapsulation, likely worse than doing nothing at all. The tube and channel designs did allow oriented tissue to grow within, but it was mostly fibrous and not neural. The tube walls essentially abutted the white matter tracts, in a similar fashion as the shells of the open-path designs. However, the tube walls were thicker than the open-path shells: 650 μm compared to 200 μm. In addition, the tube walls went all the way around and were not open. The thickness of the walls may have played a part in the switching of roles from barrier, in the tube, to guiding surface, in the open-paths. It should be noted that the tube was not representative of entubulation methods, which push cord ends into the tubes. Because we wanted to maintain a consistent implantation method, we did not make an entubulation implant though it is more commonly used, generally in combination with biological factors or cells. However, the contact guidance from an entubulating implant is solely exterior to the native SC. This type of contact is normally provided by the dura and spine and is not a cue for regeneration but a cue for enclosure. Entubulation can be considered secondary to the internal architecture, as one can use architecture encased in a tube, as with the TWC described earlier (Tsai et al., 2006). It may be beneficial to eventually incorporate both. Tubes have a tendency to collapse (Oudega et al., 2001), or pinch and obstruct cerebrospinal fluid (CSF) flow (Nomura et al., 2006) in the current animal models where laminectomy is performed on an uninjured rat. But perhaps in clinical situations, where the spine may also be damaged, a tube that encloses the SC implant may also fuse with the spine to provide bone regeneration. Interestingly, while it has been reported that axons regenerated through an entubulating implant, the stump distance reported was comparable to the stump distances measured in our study for the tube and channel designs, roughly 6—8 mm, though all started with a 4-mm defect (Tsai et al., 2004). While tissue can bridge the defect through any design, the original stumps regressed with the closed designs presented here just as with the entubulation method, in contrast to the open-path designs.

While multi-channeled scaffolds aim to increase surface areas to enhance guidance and carry trophic factors, the five channels with 450-μm diameters presented in this study did not effectively integrate with the host tissue. Channels spaced closer and with greater density may be an improvement on that design, and have shown promise when used in conjunction with cells or trophic factors (Stokols et al., 2006). But the difference in surface area occurs in conjunction with a change in architecture. In fact, though the tube and channel designs had a greater surface area, the open-path designs had a much greater effect on regeneration, further evidence that macro-architecture and targeted contact guidance are more important than total surface area.

If modifying the architecture of a non-permissive material, a PCL salt-leached sponge, can allow robust bridging and inhibition of secondary damage, the effects of biologic fac-

tors could be greatly enhanced. The use of more diverse architectures may provide a missing link in the chain of components currently being studied in SC regeneration. Applying similar principles of architecture choice based on white and gray matter delineations to other injury models like contusion or hemisection might produce designs such as those displayed in Figure 6C. Porosity could be generated by alternate methods, and different materials could be employed using the same mold.

In summary, the novel open-path designs allowed greater penetration of GFAP labeled neural tissue from both stumps and caused less scarring than the conventional implant designs. The open-path designs provided contact guidance using less material and allowed nerve fibers to extend across the entire defect length. These data suggest that implant architecture can be designed in more diverse ways to influence the regeneration of SC tissue without the use of biological factors. This study examined only architectural effects in SC transection. Future applications of these designs could include cell seeding or trophic factor impregnation. Also composite implants could enhance the guided regeneration of white matter while supporting the gray matter with cells or hydrogels infused in the core and or other specific areas of the scaffold.

Acknowledgments

Thanks go to Alex Garnepudi for all his assistance. Funding was provided by NIH (training grant T32 DE-007057-31 to D.Y.W.).

Author Disclosure Statement

No conflicting financial interests exist.

References

Bakshi, A., Fisher, O., Daggi, T., Himes, B.T., Fischer, I., and Lowman, A. (2004). Mechanically engineered hydrogel scaffolds for axonal growth and angiogenesis after transplantation in spinal cord injury. J. Neurosurg. 1, 322–329.

Barnett, S.C., and Riddell, J.S. (2007). Olfactory ensheathing cell transplantation as a strategy for spinal cord repair—what can it achieve? Nat. Clin. Pract. Neurol. 3, 152–161.

Barritt, A.W., Davies, M., Marchand, F., Hartley, R., Grist, J., Yip, P., Mcmahon, S.B., and Bradbury, E.J. (2006). Chondroitinase abc promotes sprouting of intact and injured spinal systems after spinal cord injury. J. Neurosci. 26, 10856–10867.

Busch, S.A., and Silver, J. (2007). The role of extracellular matrix in cns regeneration. Curr. Opin. Neurobiol. 17, 120–127.

Carone, T.W., and Hasenwinkel, J.M. (2006). Mechanical and morphological characterization of homogeneous and bilayered poly(2–hydroxyethyl methacrylate) scaffolds for use in cns nerve regeneration. J. Biomed. Mater. Res. Part B 78B, 274–282.

Clark, P., Connolly, P., Curtis, A.S.G., Dow, J.A.T., and Wilkinson, C.D.W. (1990). Topographical control of cell behavior. 2. Multiple grooved substrata. Development 108, 635–644.

Clark, P., Connolly, P., Curtis, A.S.G., Dow, J.A.T., and Wilkinson, C.D.W. (1991). Cell guidance by ultrafine topography *in vitro*. J. Cell Sci. 99, 73–77.

Dinh, P., Bhatia, N., Rasouli, A., Suryadevara, S., Cahill, K., and Gupta, R. (2007). Transplantation of preconditioned Schwann cells following hemisection spinal cord injury. Spine 32, 943–949.

El Maarouf, A., Petridis, A.K., and Rutishauser, U. (2006). Use of polysialic acid in repair of the central nervous system. Proc. Natl. Acad. Sci. U.S.A. 103, 16989–16994.

Flynn, L., Dalton, P.D., and Shoichet, M.S. (2003). Fiber ternplating of poly(2–hydroxyethyl methacrylate) for neural tissue engineering. Biomaterials 24, 4265–4272.

Friedman, J.A., Windebank, A.J., Moore, M.J., Spinner, R.J., Currier, B.L., and Yaszemski, M.J. (2002). Biodegradable polymer grafts for surgical repair of the injured spinal cord. Neurosurgery 51, 742–751.

Fukunaga, S., Sasaki, S., Fu, T., Yokoyama, H., Lee, I., Nakagaki, I., Hori, S., Tateishi, H., and Maruo, S. (2004). Experimental study of neural repair of the transected spinal cord using peripheral nerve graft. J. Orthop. Sci. 9, 605–612.

Gelain, F., Lomander, A., Vescovi, A.L., and Zhang, S.G. (2007). Systematic studies of a self-assembling peptide nanofiber scaffold with other scaffolds. J. Nanosci. Nanotechnol. 7, 424–434.

Goldner, J.S., Bruder, J.M., Li, G., Gazzola, D., and Hoffman-Kim, D. (2006). Neurite bridging across micropatterned grooves. Biomaterials 27, 460–472.

Hadlock, T., and Sundback, C. (2006). Biologically inspired approaches to drug delivery for nerve regeneration. Expert Opin. Biol. Ther. 6, 1105–1111.

Horn, E.M., Beaumont, M., Shu, X.Z., Harvey, A., Prestwich, G.D., Horn, K.M., Gibson, A.R., Preul, M.C., and Panitch, A. (2007). Influence of cross-linked hyaluronic acid hydrogels on neurite outgrowth and recovery from spinal cord injury. J. Neurosurg. 6, 133–140.

Houle, J.D., and Ziegler, M.K. (1994). Bridging a complete transection lesion of adult-rat spinal-cord with growth factor—treated nitrocellulose implants. J. Neural Transplant. Plast. 5, 115–124.

Houle, J.D., Tom, V.J., Mayes, D., Wagoner, G., Phillips, N., and Silver, J. (2006). Combining an autologous peripheral nervous system "Bridge" and matrix modification by chondroitinase allows robust, functional regeneration beyond a hemisection lesion of the adult rat spinal cord. J. Neurosci. 26, 7405–7415.

Huang, Y.C., Huang, Y.Y., Huang, C.C., and Liu, H.C. (2005). Manufacture of porous polymer nerve conduits through a lyophilizing and wire-heating process. J. Biomed. Mater. Res. Part B 74B, 659–664.

Hurtado, A., Moon, L.D.F., Maquet, V., Blits, B., Jerome, R., and Oudega, M. (2006). Poly(D,L-lactic acid) macroporous guidance scaffolds seeded with schwann cells genetically modified to secrete a bi-functional neurotrophin implanted in the completely transected adult rat thoracic spinal cord. Biomaterials 27, 430–442.

Ito, Y. (1999). Surface micropatterning to regulate cell functions. Biomaterials 20, 2333–2342.

Jones, L.L., Sajed, D., and Tuszynski, M.H. (2003). Axonal regeneration through regions of chondroitin sulfate proteoglycan deposition after spinal cord injury: a balance of permissiveness and inhibition. J. Neurosci. 23, 9276–9288.

Kaegi, S., Schwab, M.E., Dietz, V., and Fouad, K. (2002). Electromyographic activity associated with spontaneous functional recovery after spinal cord injury in rats. Eur. J. Neurosci. 16, 249–258.

Kuo, H.S., Tsai, M.J., Huang, M.C., Huang, W.C., Lee, M.J., Kuo, W.C., You, L.H., Szeto, K.C., Tsai, I.L., Chang, W.C., Chiu, C.W., Ma, H., Chak, K.F., and Cheng, H. (2007). The combination of peripheral nerve grafts and acidic fibroblast growth factor enhances arginase i and polyamine spermine expression in transected rat spinal cords. Biochem. Biophys. Res. Commun. 357, 1–7.

Levi, A.D.O., Dancausse, H., Li, X.M., Duncan, S., Horkey, L., and Oliviera, M. (2002). Peripheral nerve grafts promoting

central nervous system regeneration after spinal cord injury in the primate. J. Neurosurg. 96, 197–205.

Li, X.G., Yang, Z.Y., and Yang, Y. (2006). Studies on repairing of hemisected thoracic spinal cord of adult rats by using a chitosan tube filled with alginate fibers. Prog. Nat. Sci. 16, 1051–1055.

Maier, I.C., and Schwab, M.E. (2006). Sprouting, regeneration and circuit formation in the injured spinal cord: factors and activity. Phil. Trans. R. Soc. B 361, 1611–1634.

Miller, C., Jeftinija, S., and Mallapragada, S. (2002). Synergistic effects of physical and chemical guidance cues on neurite alignment and outgrowth on biodegradable polymer substrates. Tissue Eng. 8, 367–378.

Mori, S. (1992). Neuronal constituents of postural and locomotor control-systems and their interactions in cats. Brain Dev. 14, S109–S120.

Noga, B.R., Kriellaars, D.J., and Jordan, L.M. (1991). The effect of selective brain-stem or spinal-cord lesions on treadmill locomotion evoked by stimulation of the mesencephalic or pontomedullary locomotor regions. J. Neurosci. 11, 1691–1700.

Nomura, H., Tator, C.H., and Shoichet, M.S. (2006). Bioengineered strategies for spinal cord repair. J. Neurotrauma 23, 496–507.

Nomura, H., Katayama, Y., Shoichet, M.S., and Tator, C.H. (2006). Complete spinal cord transection treated by implantation of a reinforced synthetic hydrogel channel results in syringomyelia and caudal migration of the rostral stump. Neurosurgery 59, 183–192.

Novikova, L.N., Novikov, L.N., and Kellerth, J.O. (2003). Biopolymers and biodegradable smart implants for tissue regeneration after spinal cord injury. Curr. Opin. Neurol. 16, 711–715.

Oudega, M., Vargas, C.G., Weber, A.B., Kleitman, N., and Bunge, M.B. (1999). Long-term effects of methylprednisolone following transection of adult rat spinal cord. Eur. J. Neurosci. 11, 2453–2464.

Oudega, M., Gautier, S.E., Chapon, P., Fragoso, M., Bates, M.L., Parel, J.M., and Bunge, M.B. (2001). Axonal regeneration into schwann cell grafts within resorbable poly(alpha-hydroxyacid) guidance channels in the adult rat spinal cord. Biomaterials 22, 1125–1136.

Patist, C.M., Mulder, M.B., Gautier, S.E., Maquet, V., Jerome, R., and Oudega, M. (2004). Freeze-dried poly(D,L-lactic acid) macroporous guidance scaffolds impregnated with brain-derived neurotrophic factor in the transected adult rat thoracic spinal cord. Biomaterials 25, 1569–1582.

Schucht, P., Raineteau, O., Schwab, M.E., and Fouad, K. (2002). Anatomical correlates of locomotor recovery following dorsal and ventral lesions of the rat spinal cord. Exp. Neurol. 176, 143–153.

Schwab, J.M., Brechtel, K., Mueller, C.A., Failli, V., Kaps, H.P., Tuli, S.K., and Schluesener, H.J. (2006). Experimental strategies to promote spinal cord regeneration—an integrative perspective. Prog. Neurobiol. 78, 91–116.

Schwab, M.E. (2002). Repairing the injured spinal cord. Science 295, 1029–1031.

Stokols, S., Sakamoto, J., Breckon, C., Holt, T., Weiss, J., and Tuszynski, M.H. (2006). Templated agarose scaffolds support linear axonal regeneration. Tissue Eng. 12, 2777–2787.

Tate, M.C., Shear, D.A., Hoffman, S.W., Stein, D.G., Archer, D.R., and Laplaca, M.C. (2002). Fibronectin promotes survival and migration of primary neural stem cells transplanted into the traumatically injured mouse brain. Cell Transplant. 11, 283–295.

Teng, Y.D., Lavik, E.B., Qu, X.L., Park, K.I., Ourednik, J., Zurakowski, D., Langer, R., and Snyder, E.Y. (2002). Functional recovery following traumatic spinal cord injury mediated by a unique polymer scaffold seeded with neural stem cells. Proc. Natl. Acad. Sci. U.S.A. 99, 3024–3029.

Thoenen, H. (1991). The changing scene of neurotrophic factors. Trends Neurosci. 14, 165–170.

Tsai, E.C., Dalton, P.D., Shoichet, M.S., and Tator, C.H. (2004). Synthetic hydrogel guidance channels facilitate regeneration of adult rat brainstem motor axons after complete spinal cord transection. J. Neurotrauma 21, 789–804.

Tsai, E.C., Dalton, P.D., Shoichet, M.S., and Tator, C.H. (2006). Matrix inclusion within synthetic hydrogel guidance channels improves specific supraspinal and local axonal regeneration after complete spinal cord transection. Biomaterials 27, 519–533.

Wong, D.Y., Hollister, S.J., Krebsbach, P.H., and Nosrat, C. (2007). Pcl and plga degradable polymer sponges attenuate astrocyte response
and lesion growth in acute traumatic brain injury. Tissue Eng. 13, 2515–2523.

Yoshii, S., Oka, M., Shima, M., Akagi, M., and Taniguchi, A. (2003). Bridging a spinal cord defect using collagen filament. Spine 28, 2346–2351.

Yoshii, S., Oka, M., Shima, M., Taniguchi, A., Taki, Y., and Akagi, M. (2004). Restoration of function after spinal cord transection using a collagen bridge. J. Biomed. Mater. Res. Part A 70A, 569–575.

Zhang, N., Yan, H.H., and Wen, X.J. (2005). Tissue-engineering approaches for axonal guidance. Brain Res. Rev. 49, 48–64.

Address reprint requests to:
Scott J. Hollister, Ph.D.
Biomedical Engineering
Department of Neurosurgery
University of Michigan
1101 Beal Avenue, 2149 LBME
Ann Arbor, MI 48109-2106

E-mail: scottho@umich.edu